Why Mg_2IrH_6 is Predicted to be a High Temperature Superconductor, but Ca_2IrH_6 is Not

Xiaoyu Wang,[a] Warren E. Pickett,[b] Michael Hutcheon,[c] Rohit P. Prasankumar,[c] and Eva Zurek*[a]

The X_2MH_6 family, consisting of an electropositive cation X^{n+} and a main group metal M octahedrally coordinated by hydrogen, Herein, we analyze the electronic structure of two members of this family, Mg_2IrH_6 and Ca_2IrH_6, showing why the former may possess superconducting properties rivaling those of the cuprates, whereas the latter does not. Within Mg_2IrH_6 the vibrations of the IrH_6^{4-} anions are key for the superconducting mechanism, and they induce coupling in the e_g^* set , which are antibonding between the H 1s and the Ir $d_{x^2-y^2}$ or d_{z^2} orbitals. Because calcium possesses low-lying d-orbitals, $e_g^* \rightarrow$ Ca d back-donation is preferred, quenching the superconductivity. Our analysis explains why high critical temperatures were only predicted for second or third row X metal atoms, and may in other systems where the antibonding anionic states are filled.

The theory-guided quest for hydride-based high-temperature conventional superconductors [1] has led to the prediction of numerous systems belonging to the class of superhydrides (*e.g.* CaH_4 [2,3] and MgH_4 [4], CaH_6 [2] and MgH_6 [5], Li_2CaH_{16} [6] and Li_2MgH_{16} [7]). Some of these binary, simple systems, stable only at high pressures, have been synthesized and their record breaking superconducting critical temperatures, T_cs, have been measured (*e.g.* CaH_6 with a reported T_c of 210-215 K at 160-172 GPa [8,9]). These successes have emboldened theoreticians to turn towards complex 1-atmosphere-metastable compounds, which are based upon hydrogen-containing molecular-building blocks, as the next set of candidates to be explored *en route* towards the ultimate goal of ambient-condition superconductivity.

A number of recent studies have used workflows that coupled high-throughput Density Functional Theory (DFT) calculations and machine-learning techniques to screen a large number of compounds as potential high-T_c candidates, followed by high-fidelity electronic structure calculations and superconducting property predictions on the most promising systems [10–15]. From these studies, a new hope has emerged as being particularly fruitful for superconductivity, based on the cubic X_2MH_6 family, where the cation X^{n+} typically represents a group 1, 2, or 13 main group metal, and M is a transition (often a noble) metal that is octahedrally coordinated by hydrogen [12–15]. Among this family, Mg_2IrH_6 has been predicted to exhibit a T_c potentially surpasses the boiling temperature of liquid nitrogen with estimates ranging from 65 K [14] to 77 K [13], and even as high as 160 K [15]. Other systems belonging to this family with predicted T_cs ranging from ∼35-80 K include Mg_2RhH_6, Mg_2PdH_6, Mg_2PtH_6 [13], Al_2MnH_6, Li_2CuH_6 [14], Na_2AgH_6, Al_2TcH_6, and Al_2ReH_6, [12]. Notably, numerous isotypic non-metallic compounds have been synthesized including Mg_2RuH_6, $NaCaIrH_6$ and Ca_2IrH_5 [16], and a pathway towards Mg_2IrH_6 via a recently synthesized Mg_2IrH_5 phase has been proposed [17].

Though these studies have computed and listed the descriptors typically associated with superconductivity, including the electron-phonon-coupling (EPC) parameter, λ, logarithmic average frequency, $\omega_{\log}$, density of states (DOS) at the Fermi level (E_F) (abbreviated as $g(E_F)$), and the superconducting gap, $\Delta_{\mathbf{k}}$, they have not analyzed the chemical features that result in high predicted T_cs for some of these compounds, but not for others. Herein, we perform such an analysis on the electronic structure of Mg_2IrH_6, which has the largest computed T_c from this family of structures, and an isotypic Ca_2IrH_6 compound, which was reported as being non-superconducting [13]. Though Mg and Ca are both group 2 elements, low-lying unoccupied d-orbitals are present in Ca but not in Mg. Our analysis shows that back-donation from the IrH_6^{4-} anion to the Ca d bands is the reason why superconductivity is quenched for Ca_2IrH_6, and we discuss the implications on superconductivity in other systems in light of these findings.

considering the molecular orbitals (MOs) of the closed-shell IrH_6^{3-} anion (Figure 1A). Because the core states of Mg ($2s^2, 2p^6$) are too low in energy, and the empty states ($3s, 3p$) are too high, the frontier MOs of this anion in the solid should contribute to the states close to E_F, and the band that crosses it. The highest occupied MO (HOMO) in IrH_6^{3-} turns out to be triply degenerate – the d_{xy}, d_{yz}, d_{xz} orbitals that point between the ligands , and do not interact with them, in accordance with predictions from ligand field theory (LFT). While LFT would suggest that the doubly degenerate e_g^* orbitals, composed from an out-of-phase combination of the $d_{x^2-y^2}$ or d_{z^2} orbitals with the hydrogen s orbitals would correspond to the lowest unoccupied MOs (LUMOs), in our molecular calculations the a_{1g}^*, an antibonding combination of the Ir 6s and H 1s orbitals, falls between the t_{2g} and e_g^* sets. Both of the e_g^* orbitals turn out to have substantial contributions on the hydrogens, and are very diffuse pointing away from the Ir-H contact owing to the antibonding interaction. To this important point, we will return below.

In Mg_2IrH_6 the anion is IrH_6^{4-}. In this molecule the excess electron would occupy the a_{1g}^* orbital, as shown in the schematic level diagram in Figure 1A. We relaxed the structure of the IrH_6^{4-} molecule with this electronic configuration, and an Ir-H bond length of 1.805 Å was ob-

[a] Dr. X. Wang, Dr. E. Zurek*
Department of Chemistry, State University of New York at Buffalo, Buffalo, New York, USA E-mail: ezurek@buffalo.edu

[b] Dr. Warren E. Pickett
Department of Physics and Astronomy, University of California Davis, Davis, California, USA

[c] Dr. M. Hutcheon, Dr. R. Prasankumar
Deep Science Fund, Intellectual Ventures, Bellevue, Washington, USA

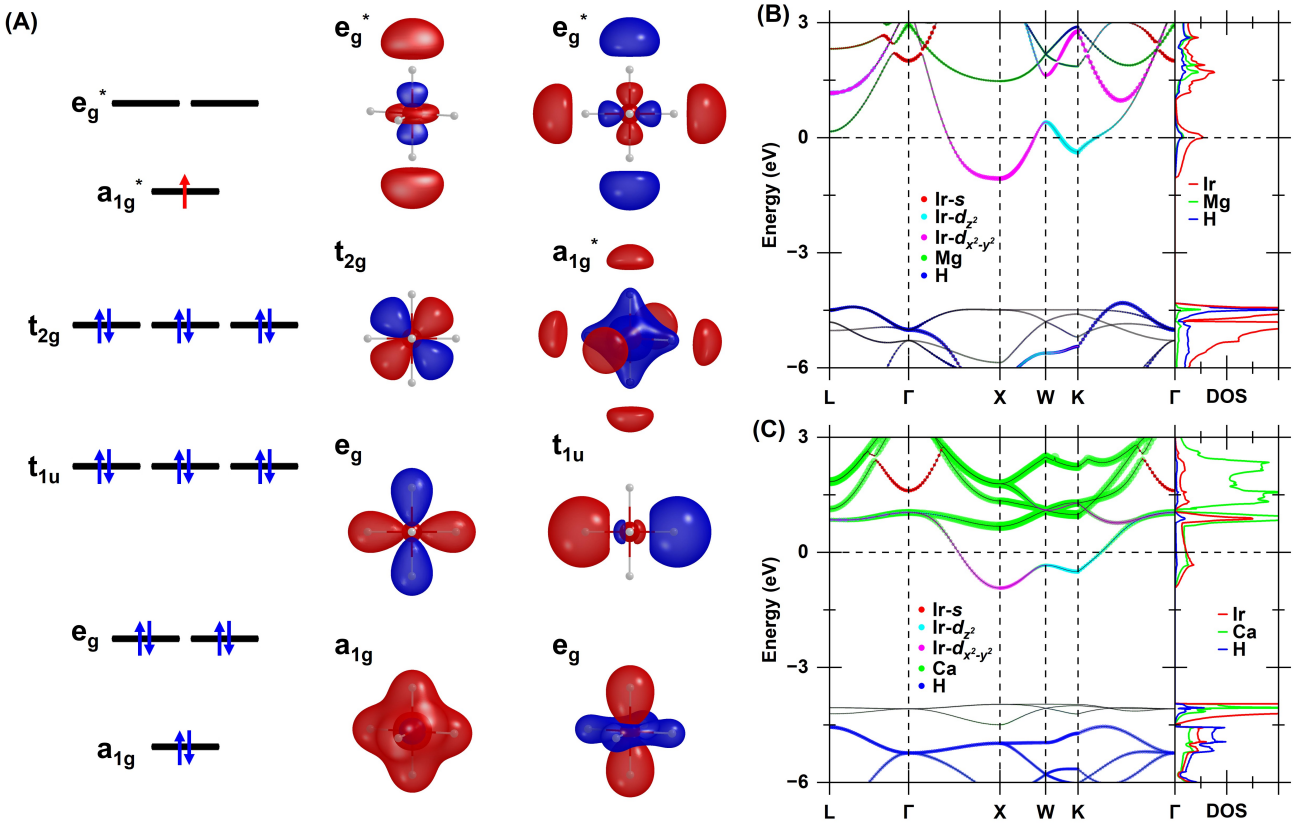

Figure 1. (A) Approximate molecular orbital (MO) diagram of IrH_6^{3-} anion (occupation shown denoted by the blue arrows), and isosurfaces of the resulting orbitals . The isovalue was chosen so that 35% of the charge is encompassed within the surface. The red arrow illustrates the electron occupation for the IrH_6^{4-} anion. Bandstructure and density of states of (B) Mg_2IrH_6 and (C) Ca_2IrH_6. The bandstructure is colored by projections onto specific Ir orbitals and the Mg/Ca/H atoms, whereas the density of states is given as atomic projections.

tained, longer than the distance within the IrH_6^{3-} molecule (1.741 Å) because the bonds are stretched when an electron fills the antibonding state. However, the Ir-H bond in the Mg_2IrH_6 crystal is unusual, 1.724 Å, which is much shorter than in molecular IrH_6^{4-}, and closer to the value found in IrH_6^{3-}. To understand why this is so, we need to account for the periodicity of the structure, and inspect the Bloch functions formed by the symmetry-adapted linear combinations of the IrH_6^{4-} MOs[18].

Though we cannot completely project the electronic bandstructure onto the MOs, we can project it onto those atomic orbitals (AOs) that contribute significantly to them. For example, projecting onto the Ir 6*s* should capture bands comprised of the a_{1g} and the a_{1g}^* MOs. The occupied a_{1g} state is far below the energy scale that we plot in Figure 1B, but the a_{1g}^*, which possesses *s*-like symmetry, has its minimum energy ∼2.5 eV above E_F at the Γ point, where it interacts in-phase with a_{1g}^* orbitals in neighboring unit cells. The next set of MOs, the e_g^*, yield two bands that can be projected onto the d_{z^2} and $d_{x^2+y^2}$ AOs of the Ir atom. Along the Γ-*L* high-symmetry line these two bands are degenerate and slightly higher in energy than a band with Mg *s*-character. Along the path, however, the d_{z^2} branch disperses below E_F, while the $d_{x^2-y^2}$ possesses a lower energy along the path. Therefore, unlike in molecular IrH_6^{4-}, where the unpaired electron fills the a_{1g}^* orbital, within the Mg_2IrH_6 crystal the excess electron fills the e_g^*-based Bloch states, explaining the aforementioned discrepancy in the bond lengths. Within PBE we find the Mg_2IrH_6 crystal relaxes to a non-magnetic ground state with a remarkably high $g(E_F)$, in-line with previous studies[13,15]. For this geometry the ferromagnetic configuration is ∼25.4 meV/atom higher in energy.

Let us now turn to the isotypic Ca_2IrH_6, which, somewhat surprisingly was not predicted to exhibit any superconductivity ($T_c \ll 0.1$ K)[13]. In this previous study, the radically different superconducting behavior of Ca_2IrH_6 was attributed to the expansion of the lattice constant (∼8% larger than in Mg_2IrH_6) that both weakens the interactions between neighboring IrH_6^{4-} units (resulting in a smaller $g(E_F)$), and leads to less disperse optical phonon modes, both which were proposed to result in a smaller λ[13]. To test this hypothesis, we calculated the T_c of Ca_2IrH_6 at 25 GPa – a pressure where its lattice constant is almost identical to that of Mg_2IrH_6 at 1 atm – but still we couldn't find superconductivity (Figure S4). We therefore concluded that the absence of superconductivity in Ca_2IrH_6 cannot be explained by its lattice constant.

Comparison of the bandstructure calculated for Ca_2IrH_6 with that of Mg_2IrH_6 reveals a number of similarities, such as the way in which the metallic band "runs"[18], but also some important differences (*c.f.* Figure 1B and C). Most notably, the metallic band contains significant Ca d_{xy}, d_{xz}, and d_{yz} character throughout, suggesting that these orbitals hybridize with the Ir d_{z^2} and $d_{x^2+y^2}$ (Figure S2 and S3), lowering the energy of the band at the *W*-point so it drops below E_F. Such hybridization of the metal-cation and the anionic states is not observed in Mg_2IrH_6. At first glance,

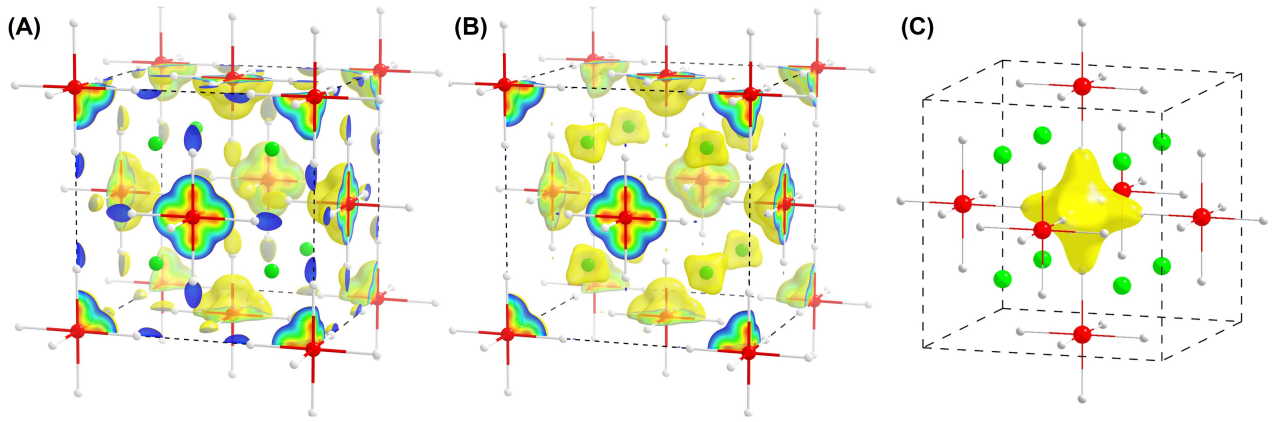

Figure 2. Charge density of the occupied metallic band calculated by integrating the charge within the energy window of $E_F - 2$ eV to E_F (the Fermi level) for (A) Mg_2IrH_6 and (B) Ca_2IrH_6. Color code for atoms: Mg/Ca-green, Ir-red, and H-white. Isovalue was chosen as in Figure 1. Color scale for contours are from blue (low density) to red (high density). (C) Isosurface of the charge density of the occupied metallic band computed on a grid that only contained points corresponding to the octahedral hole. The isovalue was chosen so that 50% of the charge is encapsulated within the surface.

this behavior is counter-intuitive: Ca has a smaller ionization potential (6.1 eV) than Mg (7.6 eV), suggesting that it should have a greater proclivity to transfer its valence electron to IrH_6^{3-}, contrary to what we observe.

Digging deeper, we can understand why this happens. The a_{1g}^* and e_g^* orbitals within IrH_6^{3-} are antibonding and it is energetically unfavorable to fill them, but in Mg_2IrH_6 there is no other choice. However, Ca contains low-lying d-orbitals available for $IrH_6^{4-} \rightarrow$ Ca d back-donation, which decreases the energy of the system. In fact, such back-donation, from H_2 σ^* orbitals to Ca d, has been noted before in theoretical studies of high-pressure hydrides including CaH_4 [3,19] and $CaSH_n$ [20]. The back-donation to the Ca-d states in Ca_2IrH_6 depletes the charge density around E_F (integration of the electron density within an energy window of $E_F \pm 0.05$ eV yielded $0.26e$/FU (formula unit) and $0.14e$/FU for Mg_2IrH_6 and Ca_2IrH_6, respectively), thereby significantly decreasing $g(E_F)$, which sits near the top of a peak in Mg_2IrH_6, but is reduced by a factor of $\sim$2 within Ca_2IrH_6.

To investigate this further, we plotted the charge density of the occupied part of the metallic band for both systems (Figure 2A and B). The topology of the IrH_6^{3-} e_g^* orbitals are evident in the plot, notably the diffuse lobes on the hydrogen atoms that are directed towards the center of an octahedron, visualized in Figure 2C. This overlap of diffuse antibonding orbitals that have a substantial contribution from hydrogen is reminiscent of the H$\leftrightsquigarrow$H bonding previously noted in metal-ammonia systems [21]. In Ca_2IrH_6, on the other hand, the lobes emanating from the hydrogen atoms are absent, and a tetrahedron of electron density surrounding each Ca atom is evident instead. This tetrahedron is consistent with the projection of the charge density onto the Ca t_{2g}^* AOs, and the placement of the metal atom within a tetrahedral hole where four neighboring IrH_6^{4-} molecules reside at the tetrahedral vertices and induce a crystal field that splits the degeneracy of the Ca 3d orbitals, which are not available for Mg. At the Γ point the t_{2g}^* orbitals are higher in energy than the e_g^* set (Figure S3), as expected from the standard two-below-three splitting observed in molecular complexes. However, in other parts of the Brillouin Zone (BZ) this energy ordering reverses, as was discussed above for the anion-centered a_g^* and e_g^* based bands. To ensure that the computed charge density for the M_2IrH_6 crystals is not a result of the self-interaction or delocalization error present within non-hybrid DFT, we recalculated the electronic structure with the range-separated hybrid HSE06 functional (Figure S1). The shape of the DOS near E_F were virtually identical (for both metal atoms), strengthening our interpretation.

Now we are ready to analyze the coupling of the Bloch functions to the lattice vibrations: the EPC behavior. We decorated the phonon dispersion curve by a red line whose thickness is proportional to the at any given wavevector $\mathbf{q}$ and phonon branch ν (Figure 3A). A at a given frequency and for a particular vibrational mode should be accompanied by a large degree of valence electron redistribution. To illustrate this point, let us focus on the phonon bands above 1250 cm^{-1} at the Γ point, because their motions can be easily described in terms of vibrations that are well known for octahedral molecules. From these, only the E_g mode (1520 cm^{-1}), which is related to the classic Jahn-Teller distortion of the IrH_6^{4-} octahedron, results in significant EPC. A single-point calculation was performed where the atoms were displaced along the eigenvectors corresponding to this mode with a displacement norm of 1 Å, resulting in the elongation of two pairs of Ir-H bonds to $\sim$1.8 Å, and the shrinking of the other pair to $\sim$1.5 Å. The charge density difference between the phonon-modulated and the unperturbed structures (ρ(modulated) $-$ ρ(unperturbed)) (Figure 3B,C) shows a concomitant redistribution of electron density with a depletion of the population of the d_{z^2}, accompanied by an increase of the $d_{x^2-y^2}$.

In contrast, neither the A_{1g} (1850 cm^{-1}) nor the T_{1u} (1444 cm^{-1}) modes induced any EPC at Γ. The highest frequency mode is the symmetric stretch of IrH_6^{4-}, which maintains its O_h symmetry, while the asymmetric T_{1u} stretch modifies the d_{z^2} and $d_{x^2-y^2}$ simultaneously. These vibrations do not break the degeneracy between d_{z^2} and $d_{x^2-y^2}$, and therefore do not induce EPC around the Γ-point, though they have non-negligible contributions in other parts of the BZ. Notably, the vibrations from adjacent IrH_6^{4-} units can modify the amount of H$\leftrightsquigarrow$H overlap in the octahedral holes (Figure 2C), whose unperturbed charge density integrates to $0.15e$ (as estimated by placing a sphere at the center with a radius of 1.14 Å) from a total of $1e$ in the occupied part

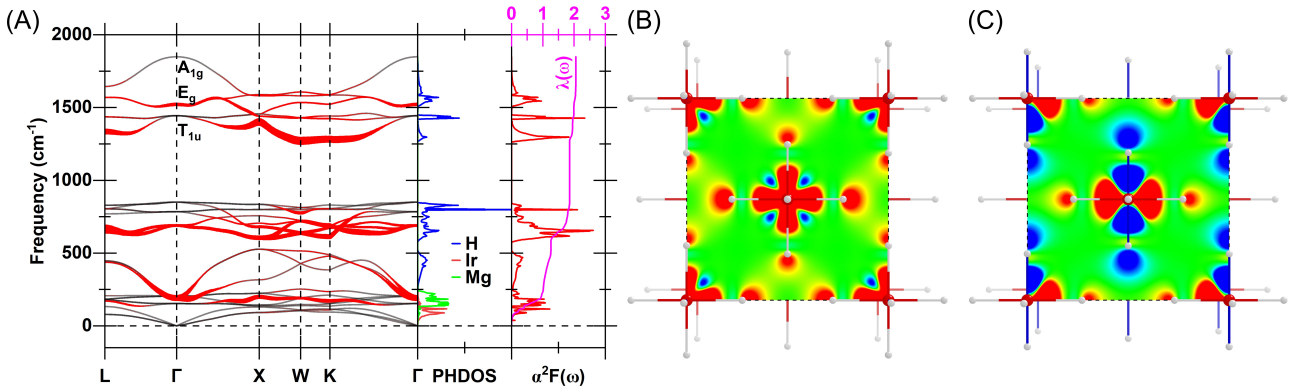

Figure 3. (A) Phonon bandstructure, projected phonon density of states, Eliashberg spectral function, $\alpha^2F(\omega)$, and integral of the electron phonon-coupling, $\lambda(\omega)$, for Mg_2IrH_6. The (B) Difference in the partial charge density for the occupied part of the metallic band between E_g-phonon-modulated structure and the unperturbed structure in the view of the xy plane and (C) yz plane. Charge gain/loss are represented with red/blue colors, while unchanged area is in green.

of the metallic band. This yields EPC throughout the BZ, and not just at Γ. The decrease in the overall $g(E_F)$, the nearly equal contribution of the Ca and IrH_6^{4-} based states to those near the Fermi level, and the heavier mass of Ca as compared to Mg are all factors that lead to a vanishingly small T_c in Ca_2IrH_6 (0.024 K in our estimate).

By comparing and contrasting the electronic structures of two isotypic structures, Mg_2IrH_6 and Ca_2IrH_6, we show why the former is predicted to be a high-T_c superconductor, whereas the latter has a T_c near 0 K. Electron donation from the electropositive metals to the antibonding molecular orbitals in IrH_6^{3-} is energetically unfavorable, and if possible, back-donation to the unoccupied low-lying metal d-orbitals is preferred instead. This back-donation is impossible for metal atoms in the second or third row of the periodic table, but can readily occur for group 1, 2 or 13 main group metals in the fourth or higher rows. Since the EPC is associated with vibrations of the molecular anion, this charge reorganization is detrimental for superconductivity. Similarly, back-donation to low-lying d-orbitals of alkaline earth metals from $H_2^{\delta-}$ σ^* [19] or $CH_4^{\delta-}$ a_1^* [23] antibonding orbitals may explain why compressed CaH_4, as well as CaC_2H_8 and SrC_2H_8 are not predicted to be good superconductors, whereas the T_cs computed for MgH_4 and MgC_2H_8 are non-negligible within their range of dynamic stability. On the other hand, back-donation to the metal d bands would not be expected when the electropositive element donates electrons to bonding or non-bonding states, for example in CaB_2 and MgB_2 where the electron fills the π-bonding states instead [24]

Our findings can explain previous results of high-throughput screening [13,14] where high T_c was only discovered when the second and the third row metals served as the electron donors (Mg_2RhH_6, Mg_2IrH_6, Mg_2PtH_6, Mg_2PdH_6, Al_2MnH_6, and Li_2CuH_6).

Acknowledgements

This work was supported by the Deep Science Fund of Intellectual Ventures and NSF award DMR-2136038. Calculations were performed at the Center for Computational Research at SUNY Buffalo (http://hdl.handle.net/10477/79221). We thank Stefano Racioppi for fruitful discussions.

Conflict of Interest

The authors declare no conflict of interest.

Data Availability Statement

Keywords: • Superconductivity • Hydrides • Electronic Structure • Density Functional Calculations • Chemical Bonding

Twitter/X Handle @ZurekThe, @UBChemistry

References

[1] K. P. Hilleke, E. Zurek, *J. Appl. Phys.* **2022**, *131*, 070901.
[2] H. Wang, J. S. Tse, K. Tanaka, T. Iitaka, Y. Ma, *Proc. Natl. Acad. Sci. U.S.A.* **2012**, *109*, 6463.
[3] A. K. Mishra, T. Muramatsu, H. Liu, Z. M. Geballe, M. Somayazulu, M. Ahart, M. Baldini, Y. Meng, E. Zurek, R. J. Hemley, *J. Phys. Chem. C* **2018**, *122*, 19370.
[4] K. Abe, *Phys. Rev. B* **2018**, *98*, 134103.
[5] X. Feng, J. Zhang, G. Gao, H. Liu, H. Wang, *RSC Adv.* **2015**, *5*, 59292.
[6] M. Redington, E. Zurek, *Chem. Mater.* **2024**, *36*, 8412.
[7] Y. Sun, J. Lv, Y. Xie, H. Liu, Y. Ma, *Phys. Rev. Lett.* **2019**, *123*, 097001.
[8] L. Ma, K. Wang, Y. Xie, X. Yang, Y. Wang, M. Zhou, H. Liu, X. Yu, Y. Zhao, H. Wang, G. Liu, Y. Ma, *Phys. Rev. Lett.* **2022**, *128*, 167001.
[9] Z. Li, X. He, C. Zhang, X. Wang, S. Zhang, Y. Jia, S. Feng, K. Lu, J. Zhao, J. Zhang, et al., *Nat. Commun.* **2022**, *13*, 2863.
[10] K. Choudhary, K. Garrity, *npj Comput. Mater.* **2022**, *8*, 244.
[11] T. F. Cerqueira, A. Sanna, M. A. Marques, *Adv. Mater.* **2024**, *36*, 2307085.
[12] T. F. Cerqueira, Y.-W. Fang, I. Errea, A. Sanna, M. A. Marques, *Adv. Funct. Mater.* **2024**, page 2404043.
[13] A. Sanna, T. F. Cerqueira, Y.-W. Fang, I. Errea, A. Ludwig, M. A. Marques, *npj Comput. Mater.* **2024**, *10*, 44.

[14] F. Zheng, Z. Zhang, Z. Wu, S. Wu, Q. Lin, R. Wang, Y. Fang, C.-Z. Wang, V. Antropov, Y. Sun, et al., *Mater. Today Phys.* **2024**, *42*, 101374.
[15] K. Dolui, L. J. Conway, C. Heil, T. A. Strobel, R. P. Prasankumar, C. J. Pickard, *Phys. Rev. Lett.* **2024**, *132*, 166001.
[16] K. Kadir, D. Moser, M. Munzel, D. Noreus, *Inorg. Chem.* **2011**, *50*, 11890.
[17] M. F. Hansen, L. J. Conway, K. Dolui, C. Heil, C. J. Pickard, A. Pakhomova, M. Mezouar, M. Kunz, R. P. Prasankumar, T. A. Strobel **2024**, arXiv preprint arXiv:2405.18544.
[18] R. Hoffmann, *Angew. Chem. Int. Ed.* **1987**, *26*, 846.
[19] T. Bi, E. Zurek, *Chem. Eur. J.* **2021**, *27*, 14848.
[20] Y. Yan, T. Bi, N. Geng, X. Wang, E. Zurek, *J. Phys. Chem. Lett.* **2020**, *11*, 9629.
[21] E. Zurek, P. P. Edwards, R. Hoffmann, *Angew. Chem. Int. Ed.* **2009**, *48*, 8198.
[22] Y. Quan, S. S. Ghosh, W. E. Pickett, *Phys. Rev. B* **2019**, *100*, 184505.
[23] N. Geng, K. P. Hilleke, F. Belli, P. K. Das, E. Zurek, *Mater. Today Phys.* **2024**, *44*, 101443.
[24] H. J. Choi, S. G. Louie, M. L. Cohen, *Phys. Rev. B* **2009**, *80*, 064503.

Entry for the Table of Contents

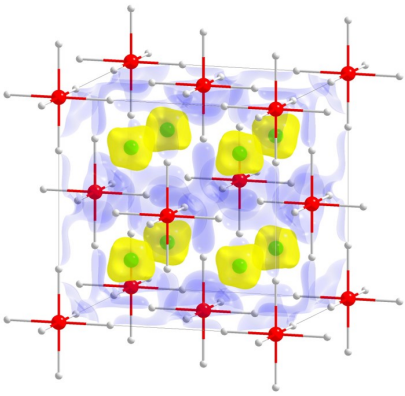

In Mg_2IrH_6, a predicted high temperature superconductor, the superconductivity results from the vibrations of the IrH_6^{4-} molecules, whose e_g^* states are found near the Fermi level. In stark contrast, in Ca_2IrH_6 superconductivity is quenched via $IrH_6^{4-} \rightarrow$ Ca d back-donation, as evidenced by a plot of the charge density of the occupied part of the metallic band, with contributions around Ca (yellow tetrahedra) and the molecular anion (blue octahedra).